Original Research Article

Effect of Cristobalite Content on Physical, Dielectric Constant, and Bending Strength of Fused Silica Ceramics Formed by Slip Casting Method

P. Dehghani [a], F. Soleimani [b] *

[a] Instructor, Department of Materials Engineering, Faculty of Engineering, University of Malayer, Malayer, Hamedan, Iran
[b] Assistant Professor, Department of Materials Engineering, Faculty of Engineering, University of Malayer, Malayer, Hamedan, Iran

A R T I C L E   I N F O

A B S T R A C T

Fused silica ceramics are widely used in electronics and aerospace industries. In the present study, 70 µm of fused silica powder was milled to 10 µm through fast milling. The appropriate slurry was prepared for slip casting with the powder-to-water ratio of 80:20. After drying the specimens, the samples were sintered at different temperatures of 1100 °C to 1400 °C. The density increased upon increasing the temperature from 1.79 to 1.98 g/cm^3. The phase transformation of the samples was investigated using XRD. The structure of the samples was analyzed using FTIR, and their microstructure was examined using a Field Emission Scanning Electron Microscope (FESEM). The bending strength of the samples was measured using the three-point method. According to the results, the cristobalite phase increased upon increasing the sintering temperature. The best flexural strength value (48.7 MPa) was obtained for the sample sintered at 1300 °C. The dielectric constants of the fused silica ceramics were about 3-3.8 in the frequency range of 8 to 12 GHz.

1. INTRODUCTION

Fused silica ceramics are among the most widely used materials in aerospace [1], laser interferometric [2], anti-reflective coating [3], investment casting [4], and capillary sensors [5]. Fused silica, also known as fused quartz, is a silica glass in an amorphous or non-crystalline form with no other additional components. Its main characteristics are low thermal expansion coefficient (0.54×10^{-6} /°C, 0-800 °C) [6], good corrosion resistance, and low dielectric constant (3-4 at 25-1000 °C), making it an attractive material [7–9].

One of the conventional methods for shaping fused silica ceramics is slip casting. Slip-cast fused silica is used to make radomes and heat shield for space rockets [10].

A key point about obtaining homogeneous and dense green bodies with uniform pore size distribution through the slip casting method is achieving a well-dispersed slurry with an appropriate particle size. Particles of 5 µm in diameter are commonly used to achieve a good mechanical strength [11]. The medium is usually water [12]; however, alcohol or methanol can also be used [13].

One of the main drawbacks of fused silica ceramics is their low flexural strength. As observed, the existence

---

* Corresponding Author Email: f-soleimani@merc.ac.ir (F. Soleimani)

and value of some Silica polymorph play a major role in the mechanical strength. The three main silica polymorphs are quartz, cristobalite, and tridymite [14,15]. Some phase transformations are diffusionless, such as β-cristobalite to α-cristobalite, meaning that the bonds do not break. Moreover, this transformation can destroy the structural integrity of the material due to volume change. The other phase transformations for fused silica, such as quartz to cristobalite, are reconstructive that tend to break bonds and reform during the transformation [16,17].

Researchers have found that conversion of amorphous fused silica to cristobalite is considered a disadvantage in their application. To be specific, based on the the literature, decrease in the bending strength during the transformation of fused silica to cristobalite is the main problem. The cubic beta crystallite is converted to alpha with a tetragonal structure. This phase change occurs at about 300 °C at a relative volume change value of 5%, which is the main reason for the formation of microcracks [18].

Some preliminary studies were conducted in early 2000 by which several researchers demonstrated the effect of incorporating small fused silica particles to the main powders while making fused silica ceramics [19]. They claimed that incorporation of some fine particles to the slurry increased the yield stress that seemed to be a reliable innovative approach to the enhancement of yield stress.

In 2016, Liu et al. [3] investigated the effect of sintering temperature on phases, microstructure, and properties of fused silica [8]. Duan et al. [7] added boron nitride to reinforced fused silica composites prepared by Hot Press (HP) at different sintering temperatures. The best dielectric results were obtained at a sintering temperature of 1350 °C, thus regarding fused silica as a high-temperature electromagnetic wave transparent material.

In the present study, the effects of sintering temperature on the density, flexural strength, and dielectric properties of fused silica ceramics were reported. Further, the amount of the cristobalite phase and its effects on the mechanical strength of the sintered fused ceramics were reported.

2. MATERIALS AND METHODS

The fused silica powder used in this experiment was purchased from the Lianyungang Hantian International Factory in China, with 99.9% purity. Table 1 presents the chemical composition of the raw material. Particle size analysis (PSA-FRITSCH) was carried out to measure the particle size. The fast mill at a speed of 120 rpm was employed to mill the fused silica powder. Alumina balls with 98% purity were also used for milling and mixing.

TABLE 1. The chemical composition of fused silica raw material

Composition	Purity%
SiO_2	99.9 %
Fe_2O_3	50 ppm
Al_2O_3	100 ppm
K_2O	42 ppm
TiO_2	17 ppm
MnO	15 ppm
P_2O_5	10 ppm

In order to prepare the sample, the weight percentage ratios of solid powders to water were claculated as 70:30, 80:20, and 90:10%. All the slurries were fast-milled for 40 h for more homogenization and mixing. After 40 h of milling, the prepared slurry passed through a 300 mesh sieve. Then, casting was conducted inside gypsum molds. The cast specimens were dried in an electric oven at 50 °C for 24 h.

After slip casting the specimens, micro cracks appeared in some cases. The sintering process was performed on the crack-free specimens. The sintering of the dried bodies was conducted at 1100, 1200, 1300, and 1400 °C. The holding time at sintering temperatures was 2 h and the heating rate was 5 °C/min.

The bulk density (ρ) and apparent porosity of the sintered samples were measured based on Archimedes method (ASTM F 417). The bending strength was measured under static, monotonic, three-point bending conditions at room temperature with the lower span of 20 mm and displacement rate of 0.5 mm/min. [20]. For this purpose, the specimens were cut in cubic segments with the dimensions of 20×28.6×1 mm and then, they were ground and polished by alumina abrasive powder.

The phase composition of the samples was determined by X-Ray Diffraction (XRD; Philips Xpert MPD Co., Ltd) using Cu Kα radiation (λ = 1.5406 Å), and their microstructures were observed through field Smission Dcanning Electron Microscopy (FE-SEM; TESCAN MIRA3). The dimensions of specimens were 10×10 mm with thickness of 5 mm. The samples were cut, polished, and etched in a 5% volumetric solution of hydrofluoric acid for 10 seconds.

The cristobalite content in the sintered samples was measured by the semi-quantitative method according to the XRD results [21] obtained from the X'Pert software. The crystalline phase values of cristobalite were calculated by measuring the intensity of the crystalline peaks relative to the 100% amorphous sample.

The structural analysis of the samples was carried out using the FTIR method. The samples were first powdered and then mixed with KBr at a ratio of 1:100; finally, the FTIR spectra were obtained.

The dielectric properties (dielectric permittivity and loss tangent) of the samples were determined by a VNA

(Keysight 5063A). The method of analysis was consistent with the waveguide method and performed in the range of the X-band [22].

3. RESULTS AND DISCUSSION

Figure 1 displays the particle size change after milling. Almost 90% of the particles were <8 microns after 40h of milling. Evidently, the milling process was good enough. In the batches, the 90:10 powder-to-water sample had very high viscosity and could not be slip cast. On the contrary, the slurry of 70:30 had very low viscosity and was not appropriate for slip casting. Therefore, the 80:20 sample was chosen for the rest of the experiments. After slip casting, it was dried and sintered at different temperatures. To assess the effectiveness of the sintering process, first, the sample densities were measured. According to the results obtained from the density measurement of the samples using the Archimedes method, upon increasing the temperature, the density of the specimens increased (Table 2). This process stopped in S28 sample and density reached its maximum value of 1.98 g/cm^3.

TABLE 2. Densities and apparent porosity of the samples

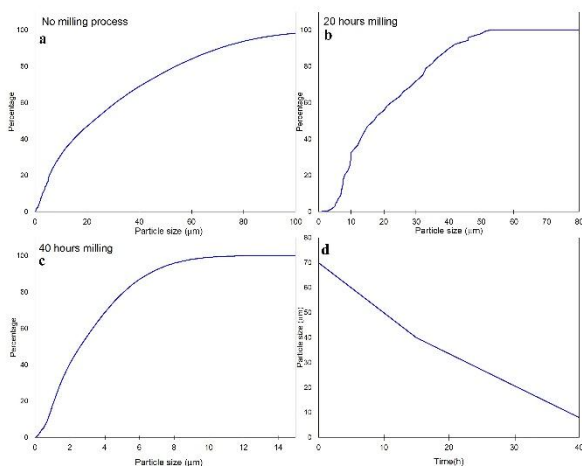| Sample Code	Density (g/cm^3)	Apparent Porosity (%)	Sintering Temperature (°C)
S22	1.79±0.05	26±0.1	1100
S24	1.96±0.05	22±0.2	1200
S26	1.98±0.05	18±0.1	1300
S28	1.98±0.05	17±0.1	1400

Figure 1. Particle size distribution of the primary powders before a) No milling, and after a different period of milling times: b) 20h milling, c) 40h milling, and d) Particle size change with milling time

Figure 2 depicts the diagram of porosity vs. bulk density. According to Figure 2, there is an inverse relationship between the temperature and apparent porosity. One of the reasons for the difference between the apparent porosity and bulk density is the phase transformation from amorphous SiO_2 to a cristobalite structure in the ceramic. To be specific, while the density of cristobalite is about 2.33 g/cm^3, it is about 2.2 g/cm^3 for silica glass. As a result, an increase in the density is due to not only porosity elimination but cristobalite crystallization, partly [23].
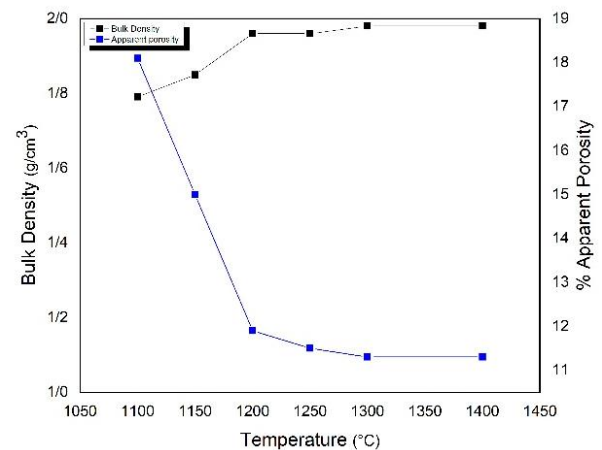

Figure 2. Relation between Bulk density, temperature, and apparent porosity in fused silica ceramics

Figure 3 depicts the images of the microstructures. According to the FESEM images in this figure, the interconnection between particles increases upon increasing the temperature. According to the FESEM images, upon increasing the sintering temperature, porosity decreases and grain sizes increase. Removing the porosity improves the dielectric constant if the cristobalite phase content is not too high. Figure 3 illustrates the formation of numerous cracks on the surface of grains in the S28 slip-cast fused silica ceramic sample. The cristobalite transformation phases usually begin from the surface of grains due to the higher heat absorption from their free surface. With an increase in the temperature from 1300 °C to 1400 °C, the grain size of particles increased and unreacted cristobalite rised. The volume changes in cristobalite after cooling at 300 °C form numerous cracks on the surface of grains, thus affecting the mechanical strength of the ceramics [24]. Whereas β-cristobalite has a cubic arrangement, α is tetragonal. The β-structure is transformed to the collapsed α structure at the ≈300 °C cooling temperature, hence occurrence of approximately a 3.2% volume reduction. The temperature of the $\propto \leftrightarrow \beta$ inversion in cristobalite is changeable which depends on the other components and crystal structure of the material.
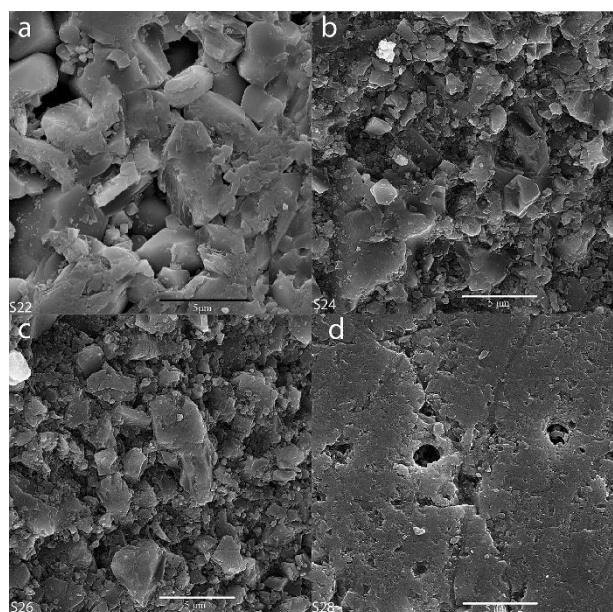
Figure 3. FESEM images of the sintered fused silica: a) S22, b) S24, c) S26, and d) S28 samples

Figure 4. XRD analysis of fused silica samples, sintered at different temperatures

Figure 4 shows the XRD diagram of fused silica ceramics. In this figure, the first peak with a higher intensity is observed at 21°, and the next two peaks with lower intensities were identified at 26° and 35°. The peaks at 21°, 26°, and 35° belong to the cristobalite phase. Cristobalite crystals are cubic in form with the chemical formula of Si_8O_{16}. Furthermore, upon increasing the temperature, the formation of the cristobalite phase begins. Evidently, no crystalline phases are observed in the samples (S22) and (S24) at 1100 °C and 1200 °C, repsectively. At 1300 °C (S26), those weak peaks belonging to the crystalline phase of cristobalite are observed. In the next sample, at 1400 °C (S28), the crystals grew more. At this temperature, the highest amount of cristobalite crystal growth is observed, as shown in Figure 4. The cristobalite crystals formed at the end of the sintering operation were converted from beta-cristobalite to alpha-cristobalite in the temperature range of 200 to 270 °C. In general, cristobalite can be divided into three categories in terms of weight: low (1-20%), medium (20-80%), and high (80-100%) [23]. Here, the sample (S28) with 38 wt% cristobalite phase content had the highest crystallization value among the sintered fused silica samples. Moreover, samples (S22) and (S26) with a crystalline phase value of < 5 wt% had the lowest value. The S24 sample contained 13 wt% of the cristobalite crystalline phase.

Figure 5 displays the FTIR diagrams. This analysis comprises a co MParison of the unsintered fused silica powder and sintered sample at 1400 °C. The sharp peaks in the diagrams are observed at 474, 796, 1100, 1400, 1634, 3130, and 3430. The peaks of 3000 and above belong to water and O-H bonds.
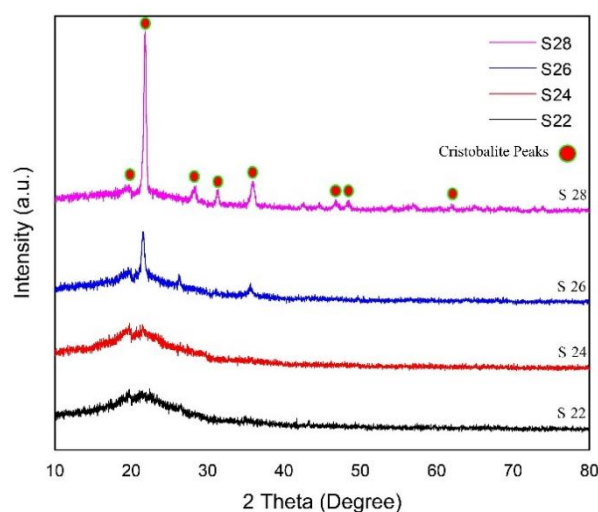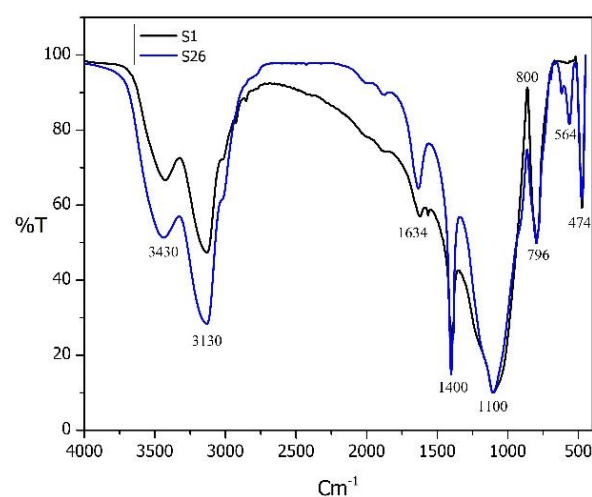

Figure 5. The FTIR analysis of fused silica powder and the sintered fused silica specimen at 1400 °C

Table 3 presents the results from the characterization of these peaks. The absorption peaks observed in the range of 800 cm^{-1} and 1080 cm^{-1} are related to Si-O vibrations in silica and those at 474 cm^{-1} to Si-O vibrations in cristobalite [14,25]. Vibrations at 1100cm^{-1} are the main structure of silica (Si-O-Si). In addition to these bond vibrations, impurities are observed in the spectroscopic diagram shown in Table 1, having smaller peaks than the original peaks. As shown in Figure 5, the peak of 564 cm^{-1} is not present in the original powder sample, and the intensity of the peaks is different in the diagrams.

The Si-O bond has a small bond length (0.162 nm) compared to the covalent radii of silicon and oxygen

(0.191 nm), which corresponds to the relatively high stability of the siloxane bond.

TABLE 3. Peaks and the type of the related bond in the FTIR analysis

Bond	Peak (cm^{-1})
Si-O bond in cristobalite	474
Si-O bond in cristobalite	621
Si-O	797
Si-OH	860
Si-O-Si	1100
(Cristobalite) Si-O	1400
OH Bond	3129, 3429

Figure 6 depicts the fracture strength diagrams of the specimens. All the specimens show brittle fracture [26]. The highest value of the fracture strength belongs to the sample (S26), which is about 49 MPa. As the sintering temperature increased to 1400 °C, the strength decreased. Due to the low sintering temperature, sample (S22) did not exhibit a good sintering behavior and, based on its density (1.79), it can be concluded that it has a high volume of porosities which reduced its mechanical strength. The maximum mechanical strength of this sample was 6.76 MPa. With an increase in the temperature to 1400 °C, the growth of the crystalline phase of cristobalite stopped, the volume change increased, and more microcracks appeared. Finally, due to the high sintering temperature and excessive growth of the cristobalite phase, the strength of fused silica ceramic after sintering at 1400 °C significantly decreased and reached 14.2 MPa.
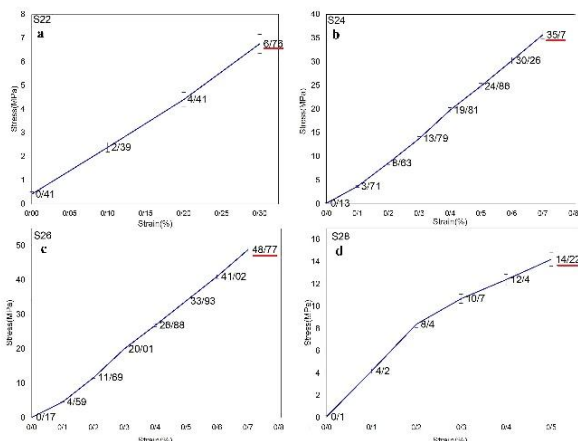

Figure 6. The bending strength of sintered fused silica specimens in the temperature range of a)1100 , b) 1200, c)1300, and d) 1400 °C

Figure 7 depicts the dielectric measurement results of the sintered samples. The dielectric constant of sample (S26) in the X-band range was 3.6, which was in agreement with the results of other studies. Evidently, samples (S24) and (S26) had the minimum noise dielectric changes. The presence of microcracks and porosities reduced the dielectric constant. Further, much noise was observed in sample (S22) due to the low density and high volume of porosities and voids. Furthermore, the low sintering temperature and less crystallized phase of cristobalite reduced the dielectric constant.

As the temperature increased, the density and porosity increased and decreased, respectively. Reduction of porosity improved the dielectric constant and eliminated noise; hence, the lowest noise was observed in samples (S24) and (S26). Upon increasing the temperature from 1200 °C to 1300 °C, the dielectric constant increased from 3.2 to 3.6.
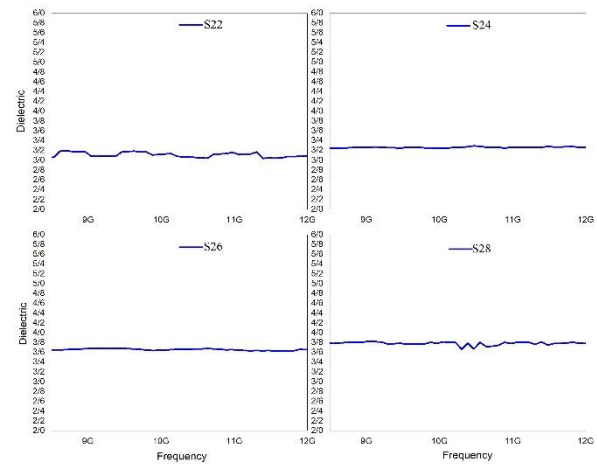

Figure 7. Dielectric constant of the samples in range of 8 to 12 GHz

Figure 8 shows the relationship between temperature and dielectric constant. With a rise in the temperature from 1100 to 1400 °C, the dielectric constant also increased. It seems that the formation of cristobalite caused an increase in the dielectric constant due to the formation of a more regular long-range structure than the amorphous phase of fused silica. The dielectric constant (ε_r) and dielectric loss increased upon increasing the grain size [27].

4. CONCLUSION

Fused silica ceramics with high density and good mechanical strength were prepared in this study. The
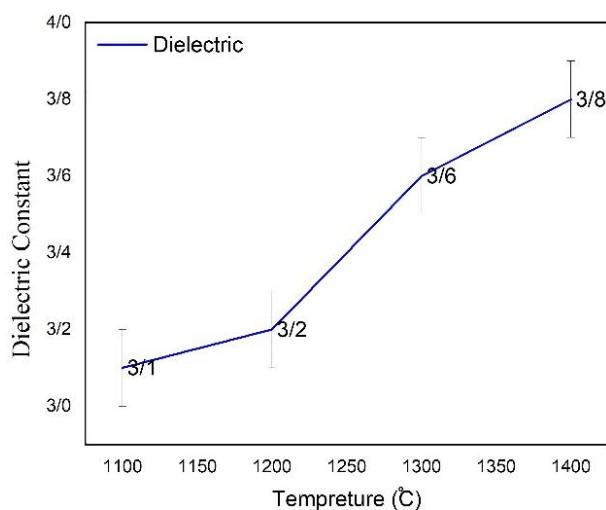
Figure 8. The relationship between dielectric and densities of the samples at the range of 1100-1400 °C

proper ratio of powder to water content in the slurry was 80:20 for good slip casing. The samples were sintered at the temperatures of 1100 to 1400 °C. It was found out that upon increasing the sintering temperature, the mechanical strength would decrease. The phase composition was studied, whose results revealed that cristobalite content would increase upon increasing the sintering temperature. The best mechanical strength and dielectric constant belonged to the sample of 1300 °C. The dielectric value of it was 3.6.

ACKNOWLEDGEMENTS

REFERENCES

1. Jeshrun Shalem, M., Devaraju, A., Karthik, K., "Synthesis and Characterization of Functionally Graded Ceramic Material for Aerospace Applications", In Reddy A., Marla D., Simic M., Favorskaya M., Satapathy S. (eds.), *Intelligent Manufacturing and Energy Sustainability. Smart Innovation, Systems and Technologies*, vol 169, Springer, Singapore, (2020), 483-488. https://doi.org/10.1007/978-981-15-1616-0_47

2. Okaji, M., Yamada, N., Nara, K., Kato, H., "Laser interferometric dilatometer at low temperatures: application to fused silica SRM 739", *Cryogenics*, Vol. 35, No. 12, (1995), 887-891. https://doi.org/10.1016/0011-2275(95)96887-R

3. Yoldas, B. E., Partlow, D. P., "Formation of broad band antireflective coatings on fused silica for high power laser applications", *Thin Solid Films*, Vol. 129, No. 1-2, (1985), 1-14. https://doi.org/10.1016/0040-6090(85)90089-6

4. Chen, X., Liu, C., Zheng, W., Han, J., Zhang, L., Liu, C., "High strength silica-based ceramics material for investment casting applications: Effects of adding nanosized alumina coatings", *Ceramics International*, Vol. 46, No. 1, (2020), 196-203. https://doi.org/10.1016/j.ceramint.2019.08.248

5. Cui, H., Zhong, R., Wang, X., Li, Z., Ling, Y., Yu, C., Chen, H., "Reassessment of the zircon Raman spectroscopic pressure sensor and application to pressure determination of fused silica capillary capsule", *Ore Geology Reviews*, Vol. 122, (2020), 103540. https://doi.org/10.1016/j.oregeorev.2020.103540

6. Deng, B., Shi, Y., Yuan, F., "Investigation on the structural origin of low thermal expansion coefficient of fused silica", *Materialia*, Vol. 12, (2020), 100752. https://doi.org/10.1016/j.mtla.2020.100752

7. Duan, W., Yang, Z., Cai, D., Zhang, J., Niu, B., Jia, D., Zhou, Y., "Effect of sintering temperature on microstructure and mechanical properties of boron nitride whisker reinforced fused silica composites", *Ceramics International*, Vol. 46, No. 4, (2020), 5132-5140. https://doi.org/10.1016/j.ceramint.2019.10.257

8. Liu, S. H., Chen, P., Xu, D. H., Yuan, Q. D., "Effects of sintering temperature on phases, microstructures and properties of fused silica ceramics", In Bao Y., Jiang D., Gong J. (eds.), *Key Engineering Materials*, *Vol. 726*, Trans Tech Publications Ltd., Switzerland, (2017), 399-403, https://doi.org/10.4028/www.scientific.net/kem.726.399

9. Romashin, A. G., Pivinskii, Y. E., "Properties of fused silica ceramics", *Refractories*, Vol. 9, No. 9-10, (1968), 590-595. https://doi.org/10.1007/bf01283506

10. Ganesh, I., Mahajan, Y. R., "Slip-Cast Fused Silica Radomes for Hypervelocity Vehicles: Advantages, Challenges, and Fabrication Techniques", *Handbook of Advanced Ceramics and Composites: Defense, Security, Aerospace and Energy Applications*, (2020), 251-317. https://doi.org/10.1007/978-3-319-73255-8_55-1

11. Richerson, D. W., Lee, W. E., *Modern Ceramic Engineering: Properties, Processing, and Use in Design*, 4th ed., CRC press, Taylor & Francis Group: Boca Raton, FL, USA, (2018). https://doi.org/10.1201/9780429488245

12. Talimian, A., Galusek, D., "Aqueous slip casting of translucent magnesium aluminate spinel: Effects of dispersant concentration and solid loading", *Ceramics International*, Vol. 45, No. 8, (2019), 10646-10653. https://doi.org/10.1016/j.ceramint.2019.02.134

13. Xu, Y., Mao, X., Fan, J., Li, X., Feng, M., Jiang, B., Lei, F., Zhang, L., "Fabrication of transparent yttria ceramics by alcoholic slip-casting", *Ceramics International*, Vol. 43, No. 12, (2017), 8839-8844. https://doi.org/10.1016/j.ceramint.2017.04.017

14. Heaney, P. J., "Chapter 1. Structure and chemistry of the low-pressure silica polymorphs", *Silica: Physical Behavior, Geochemistry, and Materials Applications*, Heaney, P. J., Prewitt, C. T., Gibbs, G. V. (eds.), Berlin, Boston: De Gruyter, (2018), 1-40. https://doi.org/10.1515/9781501509698-006

15. Carpenter, M. A., Salje, E. K., Graeme-Barber, A., Wruck, B., Dove, M. T., Knight, K. S., "Calibration of excess thermodynamic properties and elastic constant variations associated with the alpha ↔ beta phase transition in quartz", *American Mineralogist*, Vol. 83, No. 1-2, (1998), 2-22. https://doi.org/10.2138/am-1998-1-201

16. Fanderlik, I. ed., *Silica Glass and Its Application*, Elsevier, Amsterdam, The Netherlands, (2013).

17. Lakshtanov, D. L., Sinogeikin, S. V., Bass, J. D., "High-temperature phase transitions and elasticity of silica polymorphs", *Physics and Chemistry of Minerals*, Vol. 34, No. 1, (2007), 11-22. https://doi.org/10.1007/s00269-006-0113-y

18. Dai, Y., Yin, Y., Xu, X., Jin, S., Li, Y., Harmuth, H., "Effect of the phase transformation on fracture behaviour of fused silica refractories", *Journal of the European Ceramic Society*, Vol. 38, No. 16, (2018), 5601-5609. https://doi.org/10.1016/j.jeurceramsoc.2018.08.040

19. Niu, S. X., Cai, S., Tang, D. Z., Liu, X. G., Gu, G. H., Yao, J. S., Li, X., Wang, L. L., Fan, H. N., "Investigation on nano-fused silica in silica-based ceramic cores for investment casting", In Han, Y., Zhang, Q., Jiang, B. (eds.), *Materials Science Forum*,

Vol. 816, Trans Tech Publications Ltd., Switzerland, (2015), 266-270. https://doi.org/10.4028/www.scientific.net/msf.816.266

20. ASTM F417-78(1996), *Test Method for Flexural Strength (Modulus of Rupture) of Electronic-Grade Ceramics (Withdrawn 2001)*, ASTM International, West Conshohocken, PA, (1996). https://doi.org/10.1520/F0417-78R96

21. Cullity, B. D., *Elements of X-ray Diffraction*, Addison-Wesley Publishing Company Inc., Boston, (1956). https://www.eng.uc.edu/~beaucag/Classes/XRD/elementsofxray di030864mbp.pdf

22. Yuchang, Q., Qinlong, W., Fa, L., Wancheng, Z., "Temperature dependence of the electromagnetic properties of graphene nanosheet reinforced alumina ceramics in the X-band", *Journal of Materials Chemistry C*, Vol. 4, No. 22, (2016), 4853-4862. https://doi.org/10.1039/C6TC01163B

23. Wan, W., Huang, C. E., Yang, J., Zeng, J., Qiu, T., "Effect of sintering temperature on the properties of fused silica ceramics prepared by gelcasting" *Journal of Electronic Materials*, Vol. 43, No. 7, (2016), 2566-2572 (2014). https://doi.org/10.1007/s11664-014-3112-7

24. Provancher, W., Ghosh, A. K., "High Temperature Mechanical Behavior of Nb_5Si_3/Nb Laminates", *MRS Online Proceedings Library*, Vol. 364, (1994), 1071-1076. https://doi.org/10.1557/proc-364-1071

25. Koike, C., Noguchi, R., Chihara, H., Suto, H., Ohtaka, O., Imai, Y., Matsumoto, T., Tsuchiyama, A., "Infrared spectra of silica polymorphs and the conditions of their formation", *The Astrophysical Journal*, Vol. 778, No. 1, (2013), 60. https://doi.org/10.1088/0004-637x/778/1/60

26. Richerson, D. W., Lee, W. E., *Modern Ceramic Engineering: Properties, Processing, and Use in Design*, 4th ed., CRC press, New York, USA, (2018). https://doi.org/10.1201/9780429488245

27. Garbarz-Glos, B., Bąk, W., Budziak, A., Dulian, P., Lisińka-Czekaj, A., Czekaj, D., "The Application of the Mechanochemical Synthesis for the Preparation of Advanced Ceramics Based on Barium Titanate", *Archives of Metallurgy and Materials*, Vol. 65, No. 4, (2020) 1391-1396. https://doi.org/10.24425/amm.2020.133705